# Chapter 3
# Localized Surface Plasmon Resonances

Surface plasmon polaritons are propagating energy waves at a plane metallic–dielectric interface. Metallic nanoparticles supply an effective restoring force to drive electrons in an oscillating electromagnetic field. A specific resonance condition leads to a field amplification localized in the near zone inside and outside the particle. This resonance is called a localized surface plasmon resonance (LSPR).[1] In contrast to propagating SPPs, where the momentum-matching coupling techniques are employed, the LSPR can be excited by a direct illumination of electromagnetic waves on the curve surface of nanoparticles. The LSPR give rise to strongly enhanced field amplitude. The radiative decay of the LSPRs results in strongly enhanced scattering in the far field.[2] Nonradiative LSPR absorption also leads to a strong extinction at the resonance frequency. The spectral properties of the LSPRs are sensitive to the geometrical shape, dimensional sizes, and compositional materials of the nanostructure.[3]

This chapter begins by exploring the complex physical mechanisms involved in LSPRs. A quasi-static approximation is assumed in analyzing the interaction between electromagnetic waves and nanoparticles with dimensional sizes smaller than the wavelengths. This chapter also discusses the extinction efficiency and spectral properties of nanoparticles. The dielectric surroundings determine the optical properties of a nanoparticle. The subsection on spectral response focuses on the LSPRs with a variety of geometry shapes and dimensional sizes, as well as the interactions among multi-particles. The striking consequences of the resonantly enhanced absorption and scattering of nanoparticles are their fundamental applications in many fields, e.g., emission enhancement and biosensing, which are briefly introduced at the end of the chapter.

## 3.1 Localization of Electromagnetic Waves in Nanocavities and Nanoparticles

An ideal resonator formed by two parallel and perfect mirrors is adopted here to explain the localized resonance of electromagnetic waves. As shown in Fig. 3.1(a), a confined wave oscillates normally between the opposite surfaces of the metallic mirrors. The resonance modes inside the resonator are determined by the half-wavelength and the propagation length. The resonance conditions are $n(\omega) \times L = K \times \lambda/2$, where $L$ is the dimensional length of the resonator cavity, $K$ is an integer multiple, and $n(\omega)$ is the refractive index of the dielectric medium inside the cavity. This formula indicates that waves cannot be confined to arbitrary lengths less than a half-wavelength. This ideal establishment follows two assumptions: metallic mirrors are considered an ideal medium with zero skin depth, and no electromagnetic wave penetrates into the metals. Second, only the electromagnetic energy within the cavity is considered without considering the leaked energy outside the cavity. However, when the electromagnetic energy is localized within a nanocavity with dimensional sizes smaller than the wavelength, these assumptions are not valid.[4]

The skin depth of noble metals, such as gold, silver, and copper, is ~20–30 nm in the visible wavelength range. As shown in Fig. 3.1(b), when the dimensional sizes of the metallic nanoparticles are less than or comparable to the skin depth, the penetration effect of the electromagnetic wave into the metallic medium must be taken into account. The penetrating electric fields in turn drive the electrons to oscillate within the metallic medium. In such conditions, both the mechanical kinetic energy and the potential energy of the electrons in the electric field must be considered. Because the magnetic component is a relatively small amount, the electromechanical energy rather than the electromagnetic energy dominates the total energy. For an isolated metallic nanoparticle excited by an external electromagnetic field, the energy density is described by the Brillouin formula.[5]

Figure 3.2 illustrates the presentation of LSPPs surrounding metallic nanoparticles. A plane electromagnetic wave propagates along the horizontal axis and irradiates metallic nanoparticles in succession. The electric field

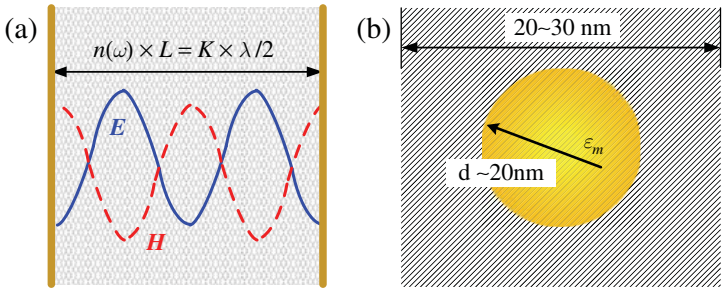


**Figure 3.1** (a) Localization of electromagnetic fields confined by an ideal resonator formed by two parallel mirrors. (b) Electric field component penetrating into a metal particle.

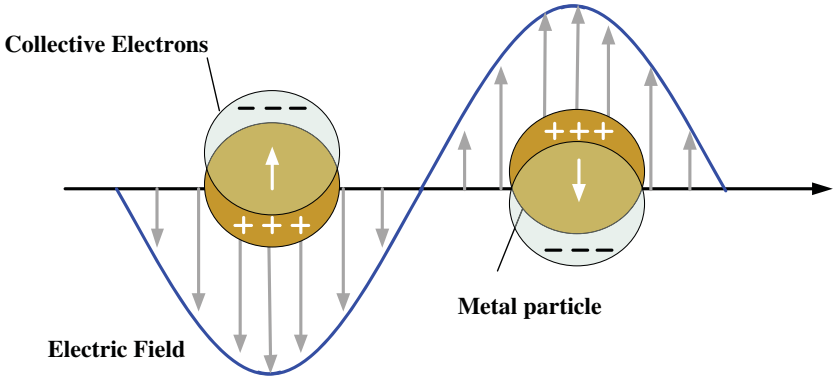


**Figure 3.2** Schematic diagrams of a localized surface plasmon occurring in two successive particles. The electron cloud deviates from its original location and accumulates at the surface of the particles.

penetrates into the metal surface and drives the electrons to deviate from their averaged equilibrium locations. The departure excites a polarization of the conduction electrons. The negative charges move toward the surface of the particle, which gives rise to a displacement of the negative charges with respect to the positive ones. The accumulation of net charges occurs at the opposite boundaries, which in turn exerts a linear restorative force on the departed electrons. The restorative force, along with the displacement vector of the electrons, attracts these charges to oscillate in an electromechanical manner. As a consequence, a dipole oscillation of the collective electrons is created by the synergetic action of both the electric field and the restorative force.[6,7]

When the oscillation frequency of a dipole approaches that of an exciting electromagnetic field, a resonance oscillation in phase leads to an enhanced local field inside and outside the nanoparticle. This collective oscillation in phase is known as a LSPR. The LSPRs can occur in spherical particles, tips, and other irregular shapes.[9]

## 3.2 Nanoparticles in a Quasi-Static Approximation

When the dimensional size of a particle is much smaller than the wavelength of the electromagnetic field, their interaction can be analyzed using the quasi-static approximation,[8] whereby the spatial field distribution around a particle can be considered as an electrostatic field over the particle volume. This approximation describes adequately the electromagnetic response of nanoparticles with dimensional sizes less than 100 nm.[1]

### 3.2.1 Quasi-static approximation

The interactions between an electromagnetic wave and a spherical particle with different dimensional sizes are shown in Fig. 3.3. When the wavelength

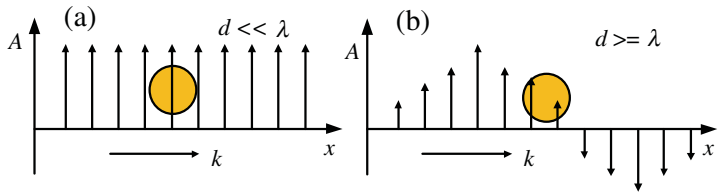


**Figure 3.3** Wave–particle interaction in the quasi-static approximation for (a) a diameter size smaller than the wavelength and (b) general cases with a diameter size greater than the wavelength.

of the exciting field is far greater than the particle diameter, as shown in Fig. 3.3(a), the electric field can be taken to be constant within the particle, although time-varying fields act on the particle volume. In this quasi-static approximation, the light–particle interaction is understood by an electrostatics assumption rather than electrodynamics. The particle maintains a homogeneous polarization due to dipole excitation. The spatial field distribution over the particle volume can be analyzed by the simply electrostatic field theory.

For the particles with greater diameters than the wavelengths, as shown in Fig. 3.3(b), the optical scattering effect becomes effective. The electromagnetic fields are spatially varying within the particle volume, which results in phase shifting in the particle due to multipole excitation, and the quasi-static approximation is no longer valid.[10]

### 3.2.2 Potentials inside the particle and the surrounding medium

In the circumstance of quasi-static approximation, the spatial field distribution can be analyzed by the electrostatic field theory. As shown in Fig. 3.4, a spherical particle with radius $d$ located at the origin point is irradiated by a polarized wave with wavelength $\lambda$. The wave propagates along the horizontal axis. If $d/\lambda < 0.1$, the polarized wave provides a uniform and static electric field $E$ over the particle volume. $\varepsilon_m$ and $\varepsilon_d$ denote the complex permittivity function of the spherical particle and the surrounding isotropic dielectric medium.

In the quasi-static approximation, the electric field is represented by a potential as $\mathbf{E} = -\nabla\mathbf{\Phi}$. The potential satisfies the Laplace equation $\nabla^2\mathbf{\Phi} = 0$.[8] As shown in Fig. 3.4(b), the Laplace equation in spherical coordinates $(r, \theta, \varphi)$ is

$$\nabla^2(r,\theta,\varphi) \times r^2 \sin\theta = \sin\theta \frac{\partial}{\partial r}\left(r^2 \frac{\partial}{\partial r}\right) + \frac{\partial}{\partial\theta}\left(\sin\theta \frac{\partial}{\partial\theta}\right) + \frac{1}{\sin\theta}\frac{\partial^2}{\partial^2\varphi}, \qquad (3.1)$$

where $r$, $\theta$, and $\phi$ are the radius, polar angle, and azimuthal angle in polar coordinates.

As shown in Fig. 3.4(a), the boundary conditions have an axial symmetry with respect to the polarization of the exciting electric field, and the exciting field is independent of an azimuth angle $\phi$. When the symmetry axis is the $z$ axis, the solution $\Phi_l(r,\theta)$ for the Laplace equation [Eq. (3.1)] is[11]

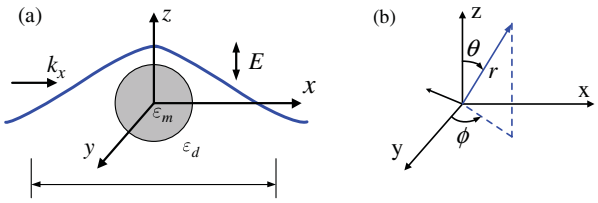


**Figure 3.4** (a) A spherical particle embedded in a surrounding dielectric medium and irradiated by a *z*-propagating, *x*-polarized wave in the quasi-static field. (b) Coordinate axes for the Cartesian and polar coordinate system.

$$\Phi_l(r,\theta) = \sum_{l=0}^{\infty}\left[A_l r^l + B_l r^{-(l+1)}\right] P_l(\cos\theta), \tag{3.2}$$

where $A_l$ and $B_l$ depend on the boundary condition of the multi-pole excitation. Because the potential remains finite at the origin, the solutions of $l = 1$ for the potentials $\Phi_m$ inside the metallic sphere and $\Phi_d$ within the dielectric medium are

$$\Phi_m(r,\theta) = A_1 r + B_1 r^{-2} P_1(\cos\theta), \tag{3.3a}$$

$$\Phi_d(r,\theta) = (B_1 r^1 + C_1 r^{-2}) P_1(\cos\theta). \tag{3.3b}$$

The potential $\Phi_d$ within the dielectric medium consists of the potentials of the incident fields and the scattered fields. The coefficients $A_1$, $B_1$, and $C_1$ are determined by the boundary conditions. At an infinite distance away from the sphere $r \to \infty$, the requirement of $\Phi_d = -E_0 r\cos\theta$ gives rise to $B_1 = -E$.

At the surface $r = d$, the tangential electric field and the normal component of the electric potential demands the boundary conditions

$$\frac{\partial\Phi_d(r,\theta)}{\partial\theta} = \frac{\partial\Phi_m(r,\theta)}{\partial\theta}, \tag{3.4a}$$

$$\varepsilon_d \frac{\partial\Phi_d(r,\theta)}{\partial r} = \varepsilon_m \frac{\partial\Phi_m(r,\theta)}{\partial r}. \tag{3.4b}$$

The incoming electric field is assumed to be homogeneous and propagate along the $x$ axis $\Phi_0 = -E_0 x = -E_0 r\cos\theta$. The evaluation of the boundary conditions leads to the potentials $\Phi_m$ inside the metallic sphere and $\Phi_d$ within the dielectric medium

$$\Phi_m(r,\theta) = -E_0 \frac{3\varepsilon_d}{\varepsilon_m + 2\varepsilon_d} r\cos\theta, \tag{3.5a}$$

$$\Phi_d(r,\theta) = -E_0 r\cos\theta + E_0 \frac{\varepsilon_m - \varepsilon_d}{\varepsilon_m + 2\varepsilon_d}\left(\frac{d}{r}\right)^3 r\cos\theta. \tag{3.5b}$$

Equation (3.5b) indicates that the potential within the dielectric medium is the superposition of the external field and an oscillating dipole field. The dipole is located at the particle's center.

### 3.2.3 Electric fields inside a particle and surrounding medium

Following the vector relationship $\mathbf{E} = -\nabla\mathbf{\Phi}$, Eqs. (3.5) give rise to the electric fields inside and outside the nanoparticle:

$$\mathbf{E}_m(r,\theta) = \mathbf{E}_0 r\cos\theta\frac{3\varepsilon_d}{\varepsilon_m + 2\varepsilon_d}, \tag{3.6a}$$

$$\mathbf{E}_d(r,\theta) = \mathbf{E}_0 r\cos\theta + \frac{\varepsilon_m - \varepsilon_d}{\varepsilon_m + 2\varepsilon_d}\left(\frac{d}{r}\right)^3\mathbf{E}_0[r\cos\theta - 3\cos\theta(\sin\theta + \cos\theta)]. \tag{3.6b}$$

In a Cartesian coordinate system, the electric field distribution [Eqs. (3.6)] is rewritten as

$$\mathbf{E}_{in}(x,y,z) = \left(\frac{3\varepsilon_d}{2\varepsilon_d + \varepsilon_m}\right)\mathbf{E}_0 k, \tag{3.7a}$$

$$\mathbf{E}_{out}(x,y,z) = \mathbf{E}_0 k - \left(\frac{\varepsilon_m - \varepsilon_d}{\varepsilon_m + 2\varepsilon_d}\right)\left(\frac{d}{r}\right)^3\mathbf{E}_0\left[k - \frac{3z}{r^2}(xi + yj + zk)\right], \tag{3.7b}$$

where $i$, $j$, $k$ denote the unit vectors in a Cartesian coordinate system, and $r$ is the distance between the origin of the coordinate system and the location of interest. The subscript *out* and *in* indicate that the fields outside and inside the particle are functions of the location, respectively, and the field distributions are not homogeneous. Equations (3.7) also indicate that the size of the nanoparticle and external dielectric permittivity function play key roles in determining the fields.

### 3.2.4 Resonance surface modes

The second term in Eqs. (3.6b) and (3.7b) describes the scattering field distribution. The scattering field looks identical to the oscillating field of a dipole locating at the origin position. The dipole moment $p$ is defined as

$$p = 4\pi\varepsilon_m d^3\frac{\varepsilon_m - \varepsilon_d}{\varepsilon_m + 2\varepsilon_d}E_0. \tag{3.8}$$

The polarizability $\chi_m$ of the dipole $p = \varepsilon_d\chi_d E_0$ induced by the external field $E_0$ is defined as

$$\chi_m = 4\pi d^3 \frac{\varepsilon_m - \varepsilon_d}{\varepsilon_m + 2\varepsilon_d}. \tag{3.9}$$

The polarizability $\chi_m$ would satisfy the resonance condition when the term $\varepsilon_m + 2\varepsilon_d$ reaches its minimum value. The imaginary part $\mathrm{Im}(\varepsilon_m)$ of most noble metals is very small and has slowly varying values with respect to the corresponding real part. In such conditions, the resonance requirement is simplified to

$$\mathrm{Re}(\varepsilon_m) = -2\varepsilon_d. \tag{3.10}$$

If the permittivity of the metallic media satisfies roughly the resonance condition, then Eqs. (3.6) and (3.7) indicate that the electric fields inside and outside the nanoparticle are enhanced relative to the incident field. The corresponding resonance frequency is $\omega_p/\sqrt{3}$. The resonance condition of nanoparticles depends on their geometries. The corresponding frequencies for various geometries are listed in Table 3.1. The resonance frequency of a bulk metal is determined by the free electron density and the effective mass. For a planar surface, the propagating SPPs are confined to the vicinity of the interface. For nanoparticles, the localized SPPs occur due to the energy confinement effects.

At a resonance mode, the electric field distribution induced by a small Au sphere embedded in an air medium can be obtained from Eqs. (3.6) and (3.7). As shown in Fig. 3.5, the enhancement factors of electric fields are normalized by the incident electric field $f_e = |E(r,0)/E_{in}|^2$ and calculated as the function of the ratio $r/d$ along the radial direction. At the spherical surface, the enhancement factor reaches sharply up to 10 and decays radically away from the interface. The electromagnetic field inside the particle remains almost invariant, whereas the intensity decays exponentially in the bulk dielectric medium away from the particle surface. This unique peculiarity is only valid in the quasi-static approximation. The particles are smaller than the skin depth of the metal.

Figure 3.6 verifies the energy localization and strong near-field intensity. At the polarized direction, the field reaches the maximum intensity and decays in the dielectric medium away from the interface. Equation (3.7) indicates that the electric field decay is proportional to $|d/r|^3$. The field intensity inside the particle remains almost constant. The arrows denote the direction and

**Table 3.1** Plasma resonances for various geometries.

| Material | Resonance Condition | Resonance Frequency |
|---|---|---|
| Bulk metal | $\varepsilon_{eff} = 0$ | $\omega_p^{Drude} = \sqrt{Ne^2/m_e\varepsilon_0}$ |
| Planar surface | $\varepsilon_{eff} = -\varepsilon_d$ | $\omega_p/\sqrt{2}$ |
| Sphere | $\varepsilon_{eff} = -2\varepsilon_d$ | $\omega_p/\sqrt{3}$ |
| Ellipsoid | $\varepsilon_{eff} = -(1 - L_m)/L_m$ | $\omega_p L_m$ |

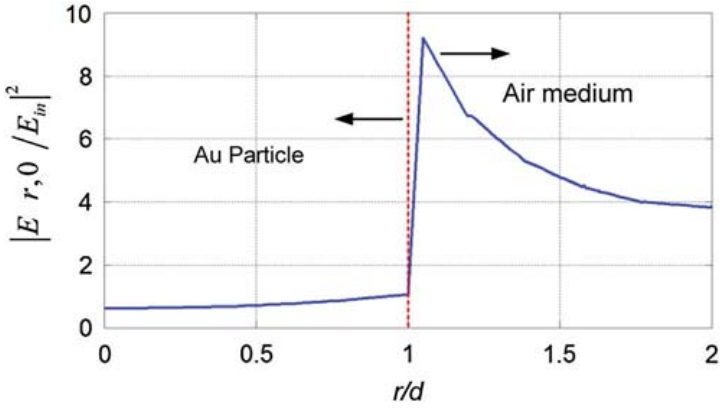


**Figure 3.5** Enhancement factors of electric fields of a gold sphere as a function of distance in the radial direction. The resonance wavelength was 639.5 nm ($\varepsilon_m = -9.51$, $\varepsilon_d = 1.09$).

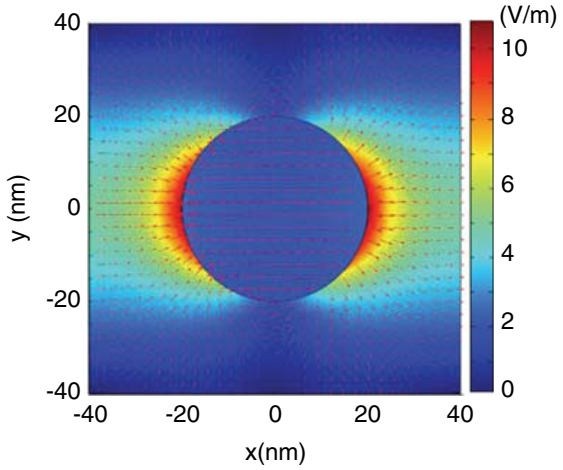


**Figure 3.6** Electric field distributions around a gold particle in a quasi-static approximation. The color map represents the field intensity, and the arrows in the logarithmic form denote the direction and magnitude of the electric field. The radius of the particle is 20 nm, and the resonance wavelength is 462 nm.

magnitude of the vector field. Both the strong field enhancement and the energy localization provide the essential for a variety of applications.[9,12]

Under the electrostatic approximation, the sizes of the particles satisfy the limit functions $x_j = k_j R << 1$, where $k_j = (2\pi/\lambda)\sqrt{\varepsilon_d(\omega)}$, $j = 0,\ 1,\ 2,\ \ldots$ denotes the order of the resonance modes, and $\varepsilon_d(\omega)$ is the dielectric permittivity of the surrounding medium. The polarization modes inside the particle are described in the equation as

$$\varepsilon_m(\omega) = -\frac{j+1}{j}\varepsilon_d, \quad j = 1,2,\ldots. \tag{3.11}$$

The polarization resonance modes within a spherical particle are schematically shown in Fig. 3.7. The lowest order $j = 1$ corresponds to a

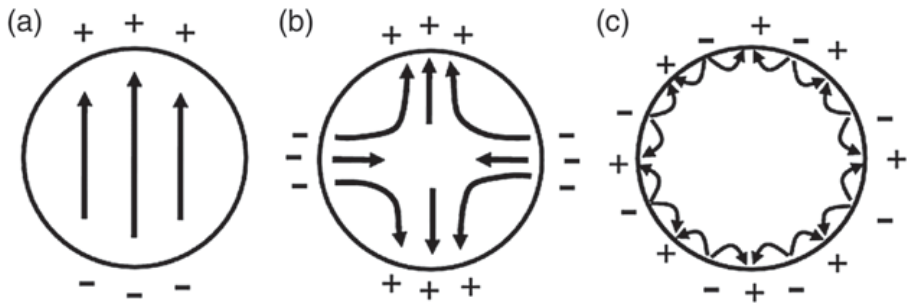


**Figure 3.7** Modes of the localized surface resonance in a sufficiently small sphere: (a) $j = 1$, (b) $j = 2$, and (c) $j \geq 3$ higher orders.

dipole fundamental mode in which the particle is polarized uniformly. The second mode $j = 2$ is a four-quadrant-pole mode. Orders greater than 2 correspond with multi-pole modes. For higher multi-pole modes, the associated electric field outside the particle decays more sharply with the increasing distance away from the sphere's surface.

### 3.2.5 Damping the plasmon resonance

Nanoparticle applications often benefit from the energy-damping effects of LSPRs.[16] The energy damping associated with the LSPRs of nanoparticles can be divided into two competing processes: a nonradiative decay process due to photonic absorption and a radiative decay process due to photonic emission.[1] As shown in Fig. 3.8, the nonradiative decay is attributed to the carrier generation that results from either intraband excitations within the conduction band or interband excitations due to the interband transitions between lower bands and the conduction band. Within noble-metal nanoparticles, the carriers appear in the form of electron–hole pairs.

Radiation decay is attributed to the direct radiation of photons into its surrounding medium from the energy system of the coherent electron oscillation. As the particle volume increases, the radiative process dominates the energy weakening. The increasing particle volume decreases the strength

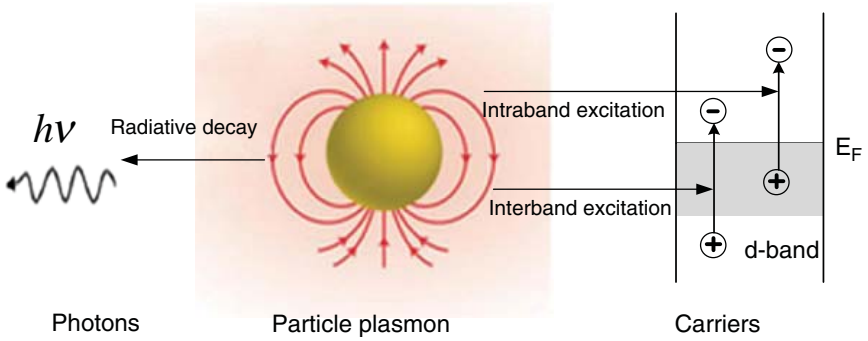


**Figure 3.8** Radiative (left) and nonradiative (right) decay process of localized surface plasmons in noble metal nanoparticles. Credit to Sönnichsen 2002.[13]

of the nonradiative decay. A radiation process will significantly broaden the resonance spectrum of the LSPRs.[13]

The relative contributions of radiative and nonradiative processes to the plasmon energy decay are important for LSPR applications of affinity biosensors. The radiative process induces the quenching of molecular fluorescence, which should dominate the identifying information.[17] The nonradiative process ultimately contributes to the sample heating in the vicinity of a metallic nanoparticle, which is useful when employing plasmonic effects to destroy tumors.[14]

## 3.3 Extinction Efficiency of Nanoparticles

The light-scattering theory of particles is divided into two categories. The first is Lord Rayleigh's theory, which is only applicable to spherical particles made of a dielectric nonabsorbing material. The second is called the Mie scattering theory, which describes a generic solution to the light scattering of spherical particles composed of absorbing or nonabsorbing materials. In particular, Mie theory describes the optical properties of metallic, spherical particles of any size.

Mie theory provides the exact solutions to Maxwell's equations to the interaction between a plane wave and a homogenous sphere. In the process of solving the equations, the optical properties of spherical particles are assumed to be the same as those of bulk metal media. The optical properties of an isolated particle and metal clusters immersed in a continuous medium have been intensively investigated in Mie scattering theory.[10,19]

### 3.3.1 Extinction efficiency in Mie theory

In the Mie theory, the extinction coefficient of spherical particles is calculated via the integration of the Poynting vector from the full electromagnetic field associated with oscillating dipoles.[18,19] The extinction properties of spherical particles are obtained from a series of multipole oscillations with appropriately specified boundary conditions. The extinction efficiency and the scattering efficiency of spherical particles with arbitrary sizes are given by

$$\sigma_{ext} = \frac{2\pi}{(k)^2}\sum_{i=1}^{\infty}(2i+1)\mathrm{Re}(a_i + b_i), \tag{3.12}$$

$$\sigma_{sca} = \frac{2\pi}{(k)^2}\sum_{i=1}^{\infty}(2j+1)\left(|a_i|^2 + |b_i|^2\right), \tag{3.13}$$

where $k$ is the wave vector of incident wavelength, and $i = 0, 1, 2, \ldots$ denotes the order of resonance modes. The extinction efficiency is the sum of scattering efficiency $\sigma_{sca}$ and absorption efficiency $\sigma_{abs}$:

$$\sigma_{ext} = \sigma_{abs} + \sigma_{sca}. \tag{3.14}$$

In Eqs. (3.12) and (3.13), $a_i$ and $b_i$ are called Mie scattering coefficients, which are functions of the particle radius and wavelength in terms of the Ricatti–Bessel spherical function [19,20]

$$a_i = \frac{\eta\psi_i(\eta x)\psi_i'(x) - \psi_i(x)\psi_i'(\eta x)}{\eta\psi_i(\eta x)\zeta_i'(x) - \zeta_i(x)\psi_i'(\eta x)}, \tag{3.15a}$$

$$b_i = \frac{\psi_i(\eta x)\psi_i'(x) - \eta\psi_i(x)\psi_i'(\eta x)}{\psi_i(\eta x)\zeta_i'(x) - \eta\zeta_i(x)\psi_i'(\eta x)}, \tag{3.15b}$$

where $\psi_i(x) \times j_i(x)$ and $\zeta_i(x) \times h_i(x)$ are the terms of the spherical Ricatti–Bessel functions, which can be found in Refs. 2 and 20. $\eta = n_m/\mathrm{Re}(n_d)$ is an equivalent refractive index of the associated material, where $n_d$ is the complex refractive index of the surrounding medium, $n_m$ is the complex refractive index of the metallic nanoparticles. The term of $n_m$ is the summation index, which includes the functions of the partial Mie extinction waves occurring inside the particle, as shown in Fig. 3.7, i.e., the dipolar oscillation mode, four-quadrant polar mode, and so on.

### 3.3.2 Electromagnetic normal modes in Mie resonances

Mie resonances in the extinction spectrum are physically interpreted by resonance conditions between the incident wave and spherical normal modes. The normal modes refer to the electromagnetic oscillations of a specific particle, which satisfy Maxwell's equations and boundary conditions at its surface.[19] The resonance conditions are expected to occur at the poles $a_i$ and $b_i$, which gives the following equations to determine the TE and TM modes[2,20]

$$TE_i \text{ modes:} \quad x_0\psi_i(x_i)\xi_i'(x_0) = x_i\xi_j(x_0)\psi_i'(x_i), \tag{3.16a}$$

$$TM_i \text{ modes:} \quad x_i\varepsilon_d\xi_i(x_0)\psi_i'(x_i) = x_0\varepsilon_m\psi_i(x_i)\xi_i'(x_0), \tag{3.16b}$$

where $x_i$ is the distance parameter

$$x_i = k_i \times R = (2\pi/\lambda_i)\sqrt{\varepsilon_d} \times R, \tag{3.17}$$

where $R$ is the radius of a nanoparticle, $\varepsilon_d$ is the dielectric function of the medium surrounding the sphere, and $k_i = (2\pi/\lambda_i)\sqrt{\varepsilon_d}$ is the wave vector of the $i = (1, 2, \ldots)$ order resonance wave with wavelength $\lambda_i$. The electric and magnetic fields associated with the $TE_i$ and $TM_i$ modes are calculated from the separate determinations of Mie scattering coefficients of $a_i$ and $b_i$.

Figure 3.9 shows the extinction spectra calculated for a silicon spherical particle and silver spherical particle embedded in an air medium, which agree well with the calculations in theory.[12] The radius of the particles are

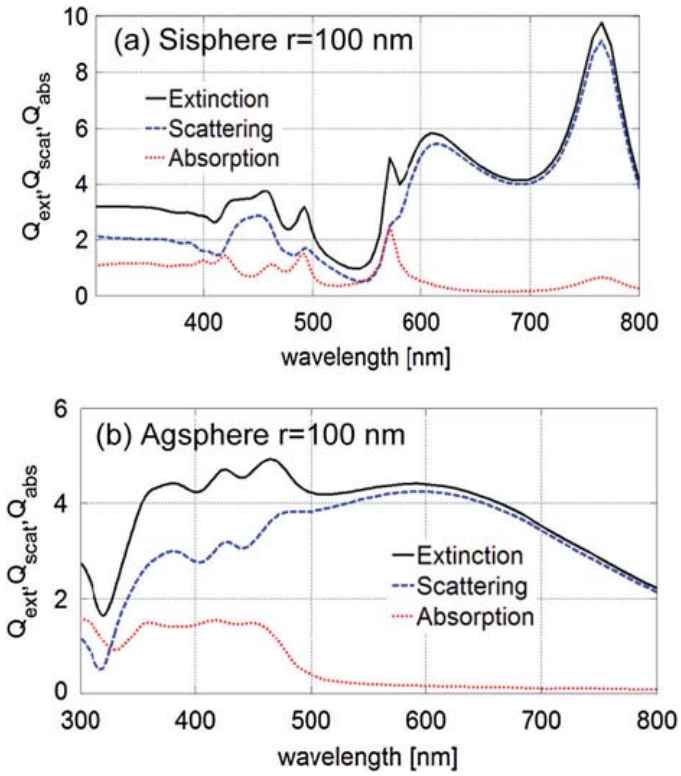


**Figure 3.9** Extinction coefficients for (a) a silicon spherical particle and (b) a silver spherical particle with a radius of 100 nm embedded in an air medium. (The light source is the total field scattered field.) The coefficients are normalized by the area of the cross-section.

100 nm. The spectra of the silicon particle exhibit both pronounced sharp and broad extinction peaks, which are associated with both $TE_j$ and $TM_j$ components. And the extinction spectra of a silver sphere appear to have relatively broad peaks relative only to the $TM_j$ modes. The modes $TM_j$ ($j = 1, 2, 3$) correspond to dipolar, four quadrant polar and higher order multipolar modes.[12] This extinction difference is attributed to the diversity of the dielectric function between the silicon and silver materials. As mentioned in Chapter 1, over the entire visible range in Fig. 3.9, the real part of the dielectric permittivity of the silicon is positive, whereas the metal silver shows negative permittivity.

### 3.3.3 Extinction efficiency for small spherical particles

In the specific case where the diameter of spherical particles satisfies the quasi-static approximation, in which the sizes of particles are much smaller than the radiation wavelength (e.g., $2r < \lambda_{max}/10$ for metallic spheres), only the dipole oscillation significantly dominates the contribution to the extinction coefficient. Under this quasi-static approximation, Mie scattering coefficients present the simple forms[2,21]

$$a_1 = -j\frac{2}{3}x^3\frac{\eta^2-1}{\eta^2+2} - j\frac{2}{5}x^5\frac{(\eta^2-2)(\eta^2-1)}{(\eta^2+2)^2} + \frac{4}{9}x^6\left[\frac{\eta^2-1}{\eta^2+2}\right]^2 + O(x^7), \quad (3.18a)$$

$$a_2 = -j\frac{2}{15}x^5\frac{(\eta^2-1)}{2\eta^2+2} + O(x^7), \quad (3.18b)$$

$$b_1 = -j\frac{1}{45}x^5(\eta^2-1) + O(x^7), \quad (3.19a)$$

$$b_2 = O(x^7), \quad (3.19b)$$

where $\eta = n_m/n_d$ is the equivalent refractive index of the medium, and $n_d$ and $n_m$ are the refractive index of the surrounding medium and the metallic medium, respectively. The size parameter is $x = (2\pi/\lambda)n_d \times R$.

The high-order terms in Eqs. (3.12) and (3.13) are ignored, and only the first term in $a_1$ is retained; the corresponding extinction coefficient for a spherical particle presents explicitly the most popular form

$$\sigma_{ext} = 9V\varepsilon_d^{3/2}\frac{\omega}{c}\frac{\varepsilon_m''(\omega)}{[\varepsilon_m'(\omega)+\chi\varepsilon_d]+[\varepsilon_m''(\omega)]^2}, \quad (3.20)$$

where $\varepsilon_m(\omega) = \varepsilon_m'(\omega) + i\varepsilon_m''(\omega)$ is the complex dielectric function of the metallic particle, $\varepsilon_d$ is the dielectric function of the surrounding medium (which is assumed to be frequency independent), and $V = (4\pi/3)R^3$ is the spherical particle volume.

Equation (3.20) indicates that the resonance condition $\varepsilon_m'(\omega) = -\chi\varepsilon_d(\omega)$ remains valid if the imaginary part $\varepsilon_m''(\omega)$ is weakly dependent on frequency. The factor $\chi$ equals 2 for the case of a sphere with a small radius. The value of factor $\chi$ can only be solved analytically for spheres and spheroids. It often approximates 3 for ellipsoid particles. When $\varepsilon_m'(\omega) = -2\varepsilon_d$ and $\varepsilon_m''(\omega)$ are independent of the frequency, a small sphere reaches roughly the localized resonance condition.

Based on the polarizability of metal spherical particles in Eq. (3.9), the scattering coefficiency is obtained by dividing the total radiated power of the exciting wave:[6]

$$\sigma_{sca} = \frac{k_d^4}{6\pi\varepsilon_0^2}|\chi_m(\omega)|^2 = \frac{8\pi}{3}k_d^4R^6\left|\frac{\varepsilon_m(\omega)-\varepsilon_d}{\varepsilon_m(\omega)+2\varepsilon_d}\right|^2. \quad (3.21a)$$

The absorption coefficiency is also obtained:

$$\sigma_{abs} = k_d\mathrm{Im}[\chi_m(\omega)] = 4\pi k_d R^3\mathrm{Im}\left[\frac{\varepsilon_m(\omega)-\varepsilon_d}{\varepsilon_m(\omega)+2\varepsilon_d}\right], \quad (3.21b)$$

where $k_d$ is the wave vector of light in the surrounding medium. Equations (3.21) indicate that both absorption and scattering are resonantly enhanced in the conditions of plasmon resonance.

The size evolution of the absorption spectra for gold spheres is shown in Fig. 3.10. The resonant peaks are located at ~530 nm with slight shifting to longer wavelengths, and the spectral width becomes broader, when the radius sizes increase. The resonant absorption of a larger diameter is much stronger than that of a smaller one. The dependence of the resonance spectra on spherical sizes is attributed to enhanced radiation damping for large particles.[19] The corresponding extinction spectra in Fig. 3.10 are calculated as shown in Fig. 3.11. It is obvious that the scattering effect plays a small role in the extinct spectra for gold spherical nanoparticles with a radius smaller than 50 nm.

The spectral properties of noble metal particles are controlled by a variety of effects, for example, the dielectric functions of the surrounding medium and the sizes and shape of the particles. The extinction spectrum of metal particles firstly depends on the dielectric function. The scattering coefficients for metallic particles embedded in varying dielectric media are calculated and shown in Fig. 3.12. The spectral peaks of silver particles are located in the ultraviolet range, whereas the maximum scattering wavelengths of gold particles are located around 530 nm. Also, the dielectric function of the surrounding media induces a slight shift of the resonance peaks. The scattering spectrum of a particle cluster with a diameter of 60 nm takes on the resonance wavelength at 566 nm for gold and 456 nm for silver.[15] The resonant wavelength of metallic particles depends on the dielectric function of the surrounding media. This property promotes the effective detection of

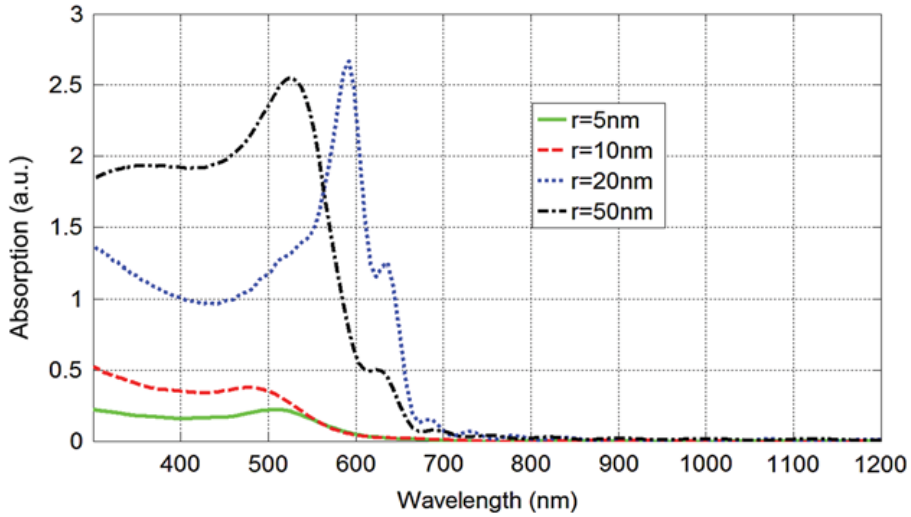


**Figure 3.10** Size effects of absorption spectra for gold spherical nanoparticles with radius sizes ranging from 5 nm to 50 nm.

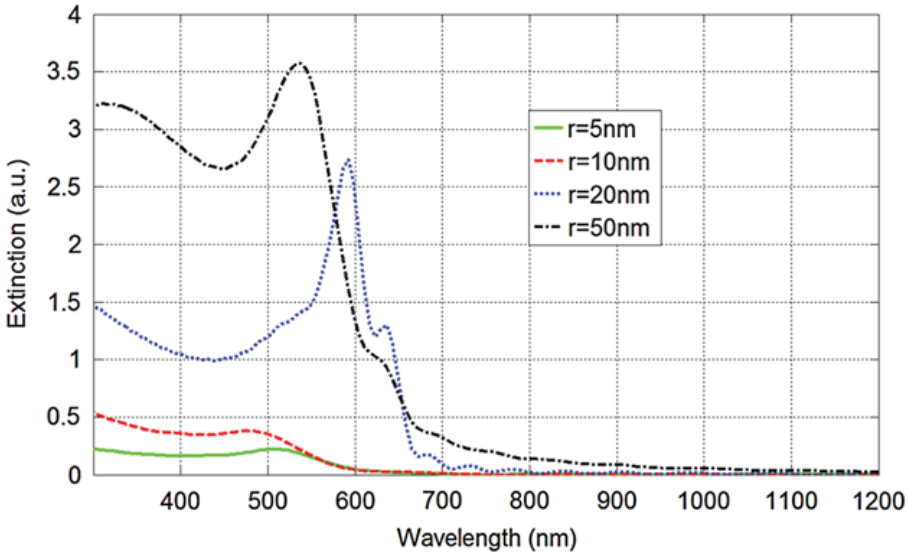


**Figure 3.11** Size effects of extinction spectra for gold spherical nanoparticles with radius sizes ranging from 5 nm to 50 nm.

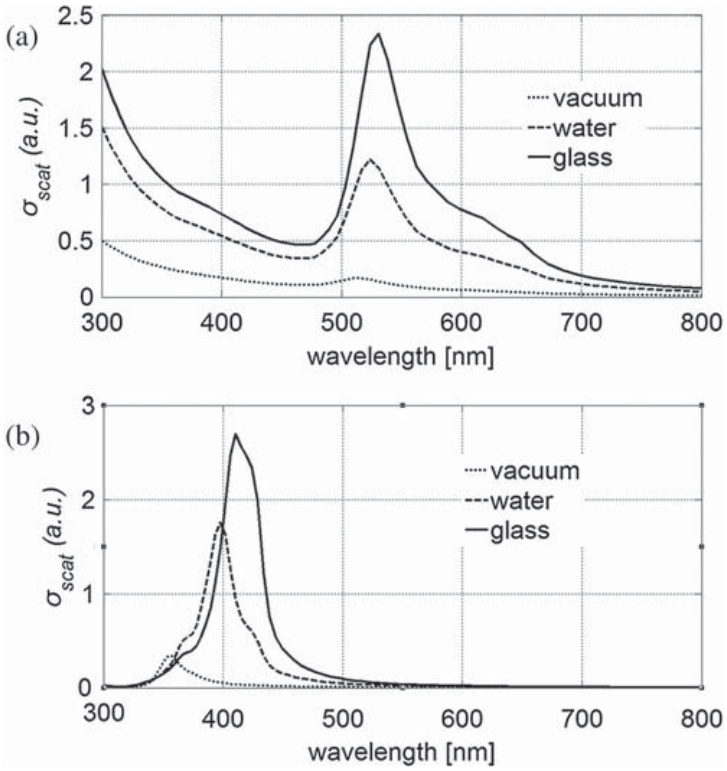


**Figure 3.12** Scattering coefficiency of spherical particles in various surrounding media for (a) gold and (b) silver. The particle radius is 5 nm. The dielectric functions of gold and silver are from Palik:[32] P295-296 (Au) and P357-358 (Ag).

solvents or adsorption of any reagent on the surface of nanoparticles. In addition, the aggregation or decentralization of nanoparticles with varying sizes will produce a pronounced frequency transition due to the resonant coupling between the illuminating waves and particles.

The mean free path effect influences the conduction electron collisions within a particle, and the optical behaviors of the metal particles. The electron mean free path of gold and silver are on the order of 30–50 nm. For metal particles with a diameter smaller than the mean free path of the conduction electrons, the particle's boundaries limit the mean free path of the conduction electrons, and the kinetic characteristics of conduction electrons are constrained by the boundaries. For the nanoparticles with a dimensional size equaling or even smaller than the electron mean free path, only the dipole term in Mie theory contribute to the extinction absorption in hypothesis. For particles with a radius on the order of or below 1 nm, the notion of a plasmon as a coherent electron oscillation breaks down, and the problem has to be treated using the quantum mechanism of a multiple-particle excitation.[19]

### 3.3.4 Extinction coefficient for large spherical particles

The extinction spectra of nanoparticles depend explicitly on their dimensional size, as discussed in Section 3.3.3. For a particle with larger dimensional sizes, the extinction specrum contains more contribution from higher-order multipolar modes. For example, a gold particle greater than ~20 nm can no longer be polarized homogeneously by an exciting field. The quasi-static approximation becomes invalid due to the significant phase shifting of the electric field through the particle volume. The inhomogeneity of the electric field within a particle induces the retardation effects, and it produces spectrum shifting and broadenings to the LSPR spectra.[7]

Given a larger sphere, the first TM mode in Mie theory is expanded to yield a spherical polarizability[24,25]

$$\chi_{sp} = V \frac{1 - \frac{1}{10}(\varepsilon_m + \varepsilon_d)\eta^2 + O(\eta^4)}{\left(\frac{1}{3} + \frac{\varepsilon_d}{\varepsilon_m - \varepsilon_d}\right) - \frac{1}{30}(\varepsilon_m + 10\varepsilon_d)\eta^2 - iV\frac{4\pi^2}{3\lambda_0^3}(\varepsilon_d)^{3/2} + O(\eta^4)}, \qquad (3.22)$$

where $\eta = \pi R/\lambda_0$ denotes an equivalent size parameter associated with the radius of particles and the free space wavelength, and $V$ is the particle volume. Unlike the expression in the quasi-static solution, the terms in the numerator and denominator lead to distinct physical significances in Eq. (3.22). The quadratic terms of the size parameter in the numerator and denominator result in a phase retardation of the electric field through the particle volume. Intuitively, increasing a particle's size will induce significant phase retardation, which will lower the resonance frequency.

The imaginary term in the denominator of Eq. (3.22) accounts for the radiation damping of the particle system. The increasing particle volume

enlarges the term of the radiation damping, which induces the strength weakening of the dipole resonance. The enlargement of the radiative damping leads to a significant broadening in the particles' resonant spectrum. In such conditions, the absorption of the nonradiative decay becomes weaker.[1]

## 3.4 Spectral Properties of Localized Surface Plasmons

### 3.4.1 Beyond the quasi-static approximation

The spectral characteristics of LSPRs include the spectral position, spectral width, and spectral height. The linewidth of a plasmonic resonance represents its lifetime broadening, which results from two damping processes. The radiation damping involves a transformation into the emission of photons and the nonradiative decay into electron-hole excitations.[13,43] As shown in Fig. 3.13, the linewidth $\Gamma$ in the extinction spectra is defined to be the full width at half maximum (FWHM), which is described quantitatively in energy units as

$$\Gamma = 2\hbar/T_2, \tag{3.23}$$

where $T_2$ is the decay time associated with the intrinsic damping processes of the collective electrons oscillation.[43,44] The decaying time relates to the population relaxation time and dephasing time:

$$\frac{1}{T_2} = \frac{1}{2T_1} + \frac{1}{T_3}, \tag{3.24}$$

where the population relaxation time $T_1$ is relevant with both the nonradiative and radiative processes, the dephasing time $T_3$ associates with the elastic loss processes.

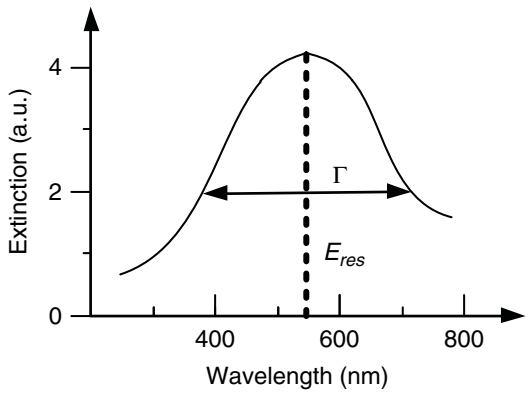


**Figure 3.13** Plasmonic linewidth is expressed using the full width at half maximum of the scattering spectra.

It is useful to maximize the quantum efficiency for resonant light scattering or to control the ratio of nonradiative and radiative population decay. To increase the radiative emission, it is advantageous to maximize the radiative contribution $T_{1,r}$ greater than the nonradiative contribution $T_{1,nr}$. A quantum efficiency is defined to quantify the light scattering as [13]

$$\eta = \frac{T_r + T_{nr}}{T_r(T_r + T_{nr})}, \tag{3.25}$$

where $T_r$ and $T_{nr}$ are the time constants for the elastic and inelastic decay of the plasmonic population. In Fig. 3.13, the LSPR strength is described by a quality factor $Q = E_{res}/\Gamma$, where $E_{res}$ denotes the resonance energy corresponding to the peak intensity.[13]

The empirical function describing the plasmonic linewidth with the radius of particle $R$ is [22]

$$\Gamma(R) = \Gamma_0 + \frac{\upsilon_F}{R} A, \tag{3.26}$$

where $\Gamma_0$ is the linewidth of the plasmonic resonances ascribed to the nonradiative damping effect. The nonradiative damping effect is dominated by the imaginary part of dielectric permittivity. $\upsilon_F$ is the Fermi velocity of metal electrons ($\upsilon_F = 1.4\times10^8$cm/s for gold). $A \approx 1$ is a relative factor in theory that incorporates the details of a scattering process, such as isotropic or diffuse scattering.[19] The linewidth relates to the lifetimes of all electron scattering processes. These scattering processes include mainly electron–electron, electron–phonon, and electron–defect scattering.

### 3.4.2 Spectrum shifting due to surrounding medium

The dielectric medium that surrounds nanoparticles induces the spectrum shifting of LSPRs. This phenomenon enables the detection of refractive index variation in environmental media, i.e., the presence of an adsorbed molecule or protein.

Let us evaluate the shifting wavelength of LSPRs due to the adsorption of a coating film in a nanoparticle surface. For an ideal particle, like that shown in Fig. 3.14, a thin coating film is adsorbed on the metal surface. The refractive index of the core particle and coating film are $n_p$ and $n_a$. The surrounding medium outside the coating film is a medium with refractive index $n_s$. The refractive indexes in the LSPR system are

$$n(x) = \begin{cases} n_p, & 0 \le x < d/2 \\ n_a, & d/2 \le x < D/2 \\ n_s, & D/2 \le x < \infty. \end{cases} \tag{3.27}$$

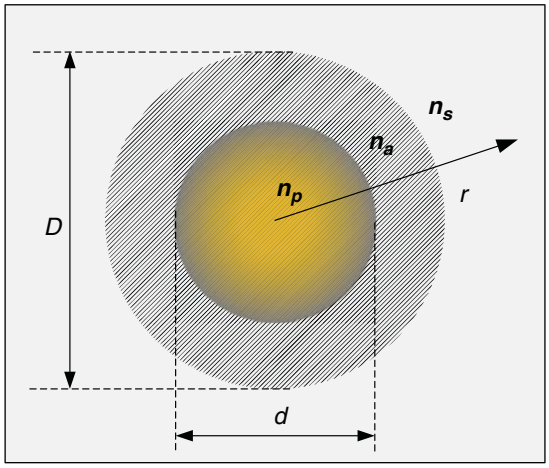


**Figure 3.14** Schematic diagram of a particle coated with an adsorption layer.

The shifting wavelength in the extinction (or scattering) spectrum of the LSPR system, ascribed to the introduction of a adsorption layer, is sensitive to the dielectric constant $n_a$ (or $\varepsilon_a$, which is related by $\varepsilon_a = n_a^2$). That is,

$$\Delta\lambda = s \times \Delta n = s \times (n_F - n_I), \tag{3.28}$$

where $s$ is the sensitivity (in nanometers per refractive index unit) of the bulk refractive index, and $\Delta n = n_F - n_I$ refers to the change of the bulk refractive index in the LSPR system. $n_I$ and $n_F$ are the bulk refractive index before and after the adsorption of the coating film in the LSPR system, respectively.

The sensitivity can be considered to be a constant factor over a narrow range of $\Delta n$. Given a small amount of shifting wavelength, the above linear relationship has been verified in both surface plasmon resonances (SPRs) and LSPRs.[9,27] However, the curvature becomes obvious for larger variation of refractive index. If higher-order terms are taken into account, their contribution is incorporated into a second-order polynomial equation:

$$\Delta\lambda = s_1 \times \Delta n + s_2 \times \Delta n^2. \tag{3.29}$$

In the absence of the coating layer, the effective refractive index $n_I$ at the initial state equals that of the surrounding medium $n_I = n_s$. However, the effective refractive index at the final state is complex because both the coating film and the surrounding medium are involved in the combination form.

The electromagnetic field around a nanoparticle depends on the spatial distance. That is, it is much stronger near the surface of the nanoparticle. The local refractive index should be properly average weighted by the intensity of the localized field over the field depth. The weighting factor is the decay field intensity $\exp(-2x/\delta_d)$. The field intensity decays in an exponential function of the distance away from the surface and a characteristic decay length $\delta_d$.[27]

Thus, the effective refractive index is integrated by the local refractive index from zero to infinity:

$$n_{eff} = \frac{2}{\delta_d}\int_0^{\infty} n(x)\exp(-2x/\delta_d)dx, \tag{3.30}$$

where $n(x)$ is the local refractive index at the location $x$ away from the particle surface. Equation (3.30) is not restricted to a trilayer structure, and it gives a general description of the effective refractive index for complex multilayer structures.

Expanding the integral in Eq. (3.30) produces

$$n_{eff} = \frac{2}{\delta_d}\left[\int_0^{D/2} n_a\exp(-2x/\delta_d)dx + \int_{D/2}^{\infty} n_s\exp(-2x/\delta_d)dx\right], \tag{3.31}$$

where $2/\delta_d$ normalizes the integration such that the condition $n_{eff} = n_s$ is valid in the absence of a coating film. The integral yields the effective refractive index of a LSPR system as

$$n_{eff} = n_s + (n_a - n_s)[1 - \exp(-D/\delta_d)]. \tag{3.32}$$

For a simple case of linear calibration in Eq. (3.29), substituting $n_{eff}$ in Eq. (3.32) into Eq. (3.28) for $n_F$ leads to

$$\Delta\lambda = s \times (n_a - n_s)[1 - \exp(-D/\delta_d)], \tag{3.33}$$

which is the shifting wavelength in a LSPR system. Equation (3.33) assumes that the shifting wavelength of a LSPR is proportional to the change in the effective refractive index of the solvent medium and the original medium. The experimental results have been verified by the full calculation using Maxwell's equations for a planar multilayer.[28,29]

Moreover, the nonlinear calibration relation in Eq. (3.29) can be adopted for bulk solutions. In such conditions, the shifting wavelength is evaluated by

$$\begin{cases} \Delta\lambda = s_1 \times \Delta n + s_2 \times \Delta n^2 \\ \Delta n = (n_a - n_s)[1 - \exp(-D/\delta_d)] \end{cases}. \tag{3.34}$$

The sensitivity factors ($s_1$, $s_2$) can be determined from a calibration process. The values are chosen to reproduce the response of a bulk refractive index.[26] The sensitivity factors in any small range of refractive indices depends on the metal nanoparticles and other parameters. In practical experiments, these sensitivity factors should be calibrated regularly.

The shifting wavelengths calculated by Eqs. (3.33) and (3.34) are the key parameters in a LSPR-based sensing measurement. This mechanism leads to a variety of chemical assays and bioassays, which probe the affinity between molecules. Following the same derivation processes, this approach

can be extended to estimate the thickness of an adsorbate, the decay depth, the refractive index of the adsorbate, and even multilayer adsorption.[26]

The performance of SPPs and LSPRs are compared by the ratio of the shifting wavelengths[8]

$$\frac{\Delta\lambda_{LSPRs}}{\Delta\lambda_{spp}} = \frac{S_{LSPRs}}{S_{spp}} \cdot \frac{\Delta n_{LSPRs}}{\Delta n_{spp}} \cdot \frac{\exp(2r/\delta_{e,spp}) - 1}{\exp(2r/\delta_{e,LSPRs}) - 1}. \tag{3.35}$$

Under the identical experimental conditions, e.g., the same metallic particle and solvent analyte, the terms $\Delta n$ of the bulk medium cancel out. The experimental results indicated that the SPPs outperform the LSPRs with respect to the sensing of the bulk refractive index. When the thickness of the adsorption layer approaches zero, the ratio in Eq. (3.35) approaches unit. The two techniques become nearly identical. However, the sensitivity of the shifting wavelength per molecule must be considered for single-molecule detection. When the area of the substrates is normalized by the number of adsorbed molecules, the performance of LSPRs will be suitable for smaller concentrations, even for single-molecule detection.[26,27]

### 3.4.3 Shape-dependent plasmon extinction spectra

The spectrum of a nanoparticle depends on a variety of effects, such as the dielectric properties of the surrounding medium and the sizes and shape of the particle. When the nanoparticles are used for sensitive detection, their sizes and shape, as well as the environmental medium, play key roles in the scattering effect. The scattering and extinction coefficiency of nonspherical nanoparticles, e.g., nanorod spheroidal particles, are very drastic effects used to quantify the analytic solutions.[2]

For metallic nanoparticles with dimensional sizes smaller than the subwavelength, the geometry and materials effects on the LSPR are shown in Fig. 3.15. When the surrounding dielectric permittivity is increased, the resonance wavelength of the extinction spectra shifts to a longer wavelength. As the aspect ratio of a nanorod particle is increased, the longitudinal resonance wavelength also shifts to a longer wavelength.[30]

Mie theory provides explanations for the spectral characteristics of randomly orientated gold nanorods.[3] The extinction coefficient of an elongated ellipsoid, given the condition of the dipole approximation, is estimated by

$$\sigma_{ext}(\lambda) = \frac{2\pi}{3\lambda} N V (\varepsilon_d)^{3/2} \sum_i \frac{(1/p_i^2)\varepsilon_m''}{\left(\varepsilon_m' + \frac{1-p_i}{p_i}\varepsilon_d\right)^2 + (\varepsilon_m'')^2}, \tag{3.36}$$

where $V$ represents the volume of the particle, $N$ is the total number of particles, and $p_i$ are the depolarization factors of nanorod particles along

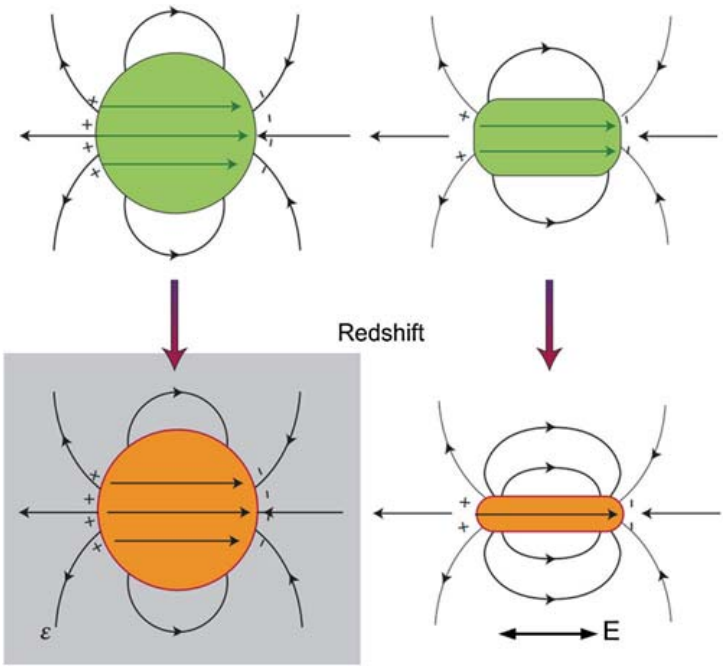


**Figure 3.15** Evolution of plasmonic resonance of metallic nanoparticles on the geometry and materials, surrounding medium and the aspect ratio. Minus (plus) signs indicate regions of high (low) electron density. Adapted from Ref. 30 with permission from Macmillan Publishers Ltd., © 2010.

three-axis Cartesian coordinates under the assumption of $R_x > R_y = R_z$. The depolarization factors are

$$p_x = \frac{1-\kappa^2}{\kappa^2}\left[\frac{1}{2\kappa}\ln\left(\frac{1+\kappa}{1-\kappa}\right) - 1\right], \tag{3.37a}$$

$$p_y = p_z = \frac{1-p_x}{2}, \tag{3.37b}$$

$$\kappa = \sqrt{1-\left(\frac{R_x}{R_y}\right)^2} = \sqrt{1-(\rho)^2}, \tag{3.37c}$$

where the aspect ratio ρ of a nanorod particle is defined as the ratio of the rod length to its width.

As shown in Fig. 3.16, the extinction coefficients for gold nanorods with a varying aspect ratio are calculated by Eq. (3.36) with the measured dielectric function.[32] The plasmon resonance of each nanorod splits into a longitudinal plasmon band and a transverse resonance, which correspond to the oscillation of free electrons along and perpendicular to the long axis, respectively. It is notable that, when the aspect ratios increase from 2.5 to 3.7, the longitudinal band is more sensitive to the nanorod aspect ratio. The longitudinal resonance

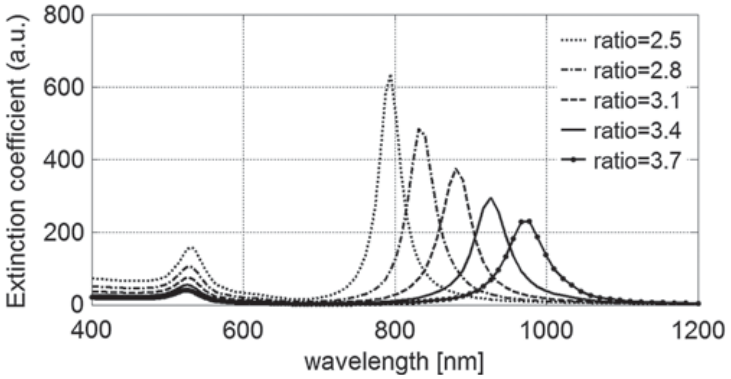


**Figure 3.16** Extinction coefficient of the localized surface plasmon of gold nanorods with varying aspect ratios. The dielectric constant was assumed to be 3.5.

continuously shifts toward the near-infrared wavelength. In contrast, the transverse resonance bands almost remain constant at ~530 nm.[42]

For the longitudinal plasmon band, Fig. 3.17 presents an approximately linear trend between the resonance wavelengths and the aspect ratios. The peak wavelengths are determined by the calculated spectra in Fig. 3.16. Considering both the aspect ratios of nanorods and the dielectric function of surrounding medium, a linear empirical formula describes the peak wavelengths of the longitudinal plasmonic spectrum,

$$\lambda_{\max} = a\varepsilon_d\rho + (b\varepsilon_d + c) = (a\rho + b)\varepsilon_d + c, \tag{3.38}$$

where $a$, $b$, and $c$ are the designated parameters. Equation (3.38) indicates that the peak wavelength of the longitudinal plasmonic modes depend linearly on the dielectric function of the surrounding medium $\varepsilon_d$ with slope efficiency $(a\rho + b)$ for a fixed aspect ratio. As the surrounding dielectric constant becomes larger, the resonance wavelength experiences a red shift. Meanwhile, for a specified surrounding medium, the peak wavelengths also depend on the aspect ratio $\rho$ with a linear slope efficiency $a\varepsilon_d$ and a constant term $(b\varepsilon_d + c)$. The peak wavelengths shift to longer wavelengths as the medium dielectric function and the aspect ratio increase.

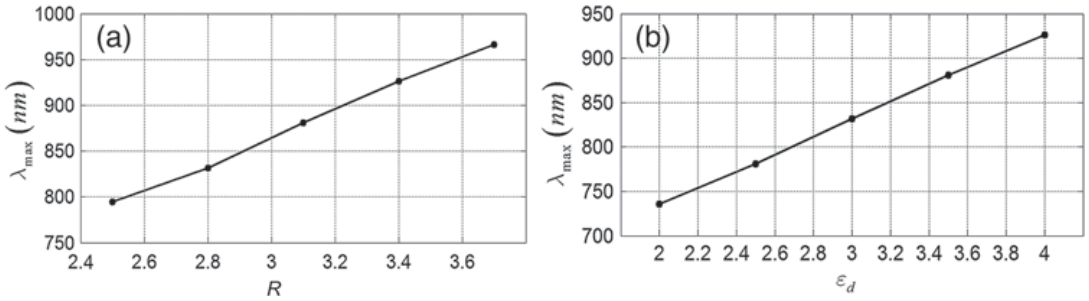


**Figure 3.17** The dependence of the peak wavelength of the longitudinal plasmon absorption for gold nanorods on (a) the aspect ratio and (b) the medium dielectric constant.

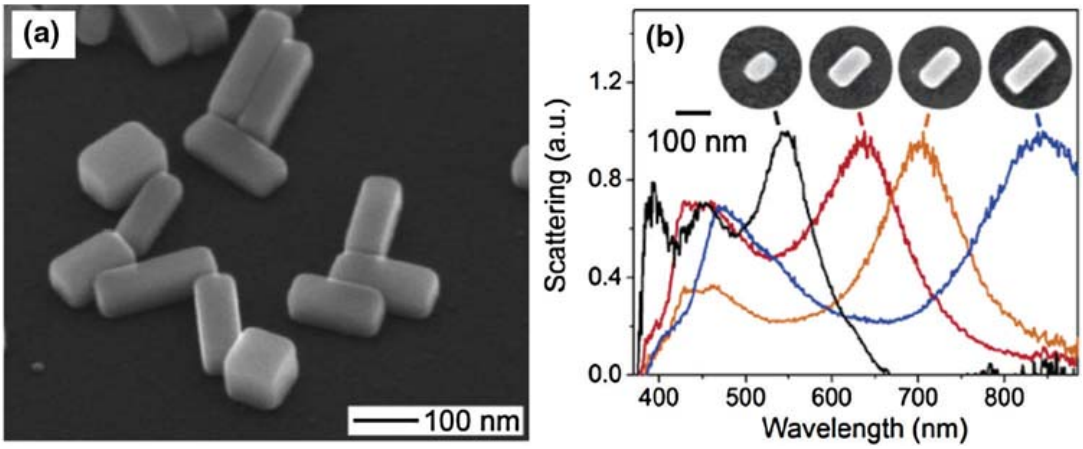


**Figure 3.18** (a) Individual silver nanobars and (b) the normalized scattering spectra. Adapted from Ref. 36 with permission from the American Chemical Society, © 2007.

Figure 3.18 shows the normalized scattering spectra of a series of silver nanobars. When the aspect ratio increases, the transverse resonance peaks remain almost constant, whereas the longitudinal resonance peaks shifts to a longer wavelength.[36]

The geometrical shape obviously affects the resonance characteristics due to the changes in surface polarization. The number of resonance absorption peaks depends on the number of polarized modes within a nanoparticle. Thus, in contrast to spherical particles, nonspherical nanoparticles exhibit multiple peaks.

Figure 3.19 shows the scattering spectra of silver particles with various shapes. The scattering spectra of an individual triangular particle, a pentagonal particle, and a spherical particle are measured.

Various shapes of nanoparticles, including spherical, cubical, tetrahedronal, octahedronal, triangular, and rectangular bars, can tailor the optical coefficients in LSPRs by the shape effect.[34] The dependence of the resonance spectral on geometrical shapes makes the nanoparticles excellent candidates for applications in near-field optical microscopy and biological assays.

## 3.5 Surface Plasmon Resonance Affinity Biosensors

For biological sensing, the adsorption of molecules on the surface of functionalized nanoparticles results in spectral shifting of the LSPR modes. The energy concentration of the LSPRs leads to fluorescence enhancement and spectrum sensitivity. These merits have allowed LSPR-affinity biosensors to become an established analytical sensing technology. In particular, the field concentration associated with a single nanoparticle has made tip-enhanced spectroscopies and other biosensors available.[8,37]

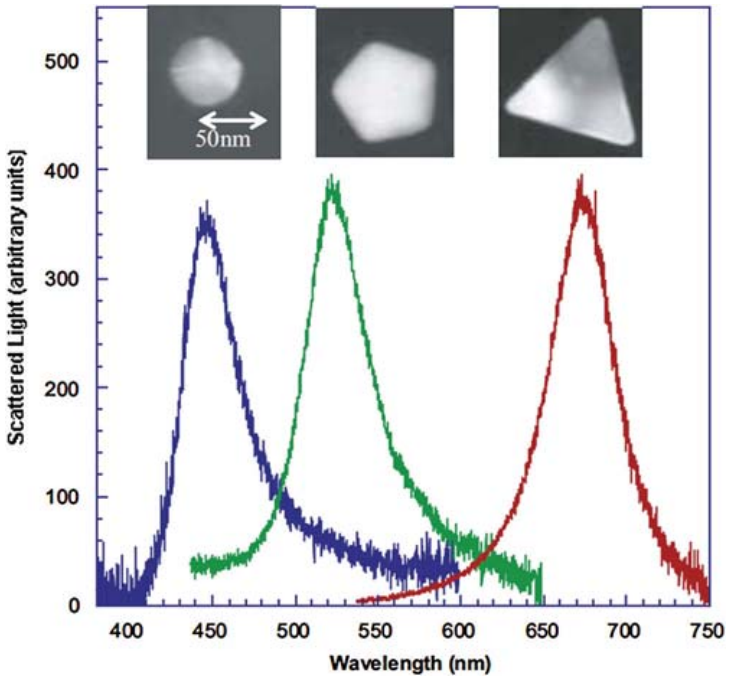


**Figure 3.19** Scattering spectra of silver nanoparticles with various shapes. Reprinted from Ref. 33 with permission from AIP Publishing, © 2002.

### 3.5.1 Fluorescence enhancement by metal nanoparticles

The enhancement effect of the electromagnetic field due to the LSPRs of metallic particles can significantly improve the fluorescent emission of dying species. A fluorescence emission is determined by the damping process, i.e., both radiative and nonradiative damping. For a molecule in contact with a metallic particle, its nonradiative transition quenches the fluorescence. It is often required that the dephasing time be slow as possible because it is advantageous to minimize the non-radiative decay and to avoid sample heating or fluorescence quenching. To obtain an enhanced fluorescence emission, a thin dielectric film is often employed to prohibit nonradiative processes.[16]

The fluorescence process is divided into two steps: fluorescence generation by the excited molecules and fluorescence modification due to the presence of a nanoparticle.[38] For a weak excitation of a single fluorescent emission, the emission coefficient $\gamma_{em}$ is related to both the excitation coefficient $\gamma_{exc}$ and the total decay coefficient:

$$\gamma_{em} = \gamma_{exc} \frac{\gamma_r}{\gamma_r + \gamma_{nr}} = \gamma_{exc} q_a, \tag{3.39}$$

where $\gamma_r$ is the radiative coefficient, $\gamma_{nr}$ is the nonradiative decay coefficient, and $q_a$ is the quantum yield of the emission.

Figure 3.20 shows the dependence of the fluorescent emission on the distance between a single fluorescent emitter and a nanoparticle. The fluorescent emission

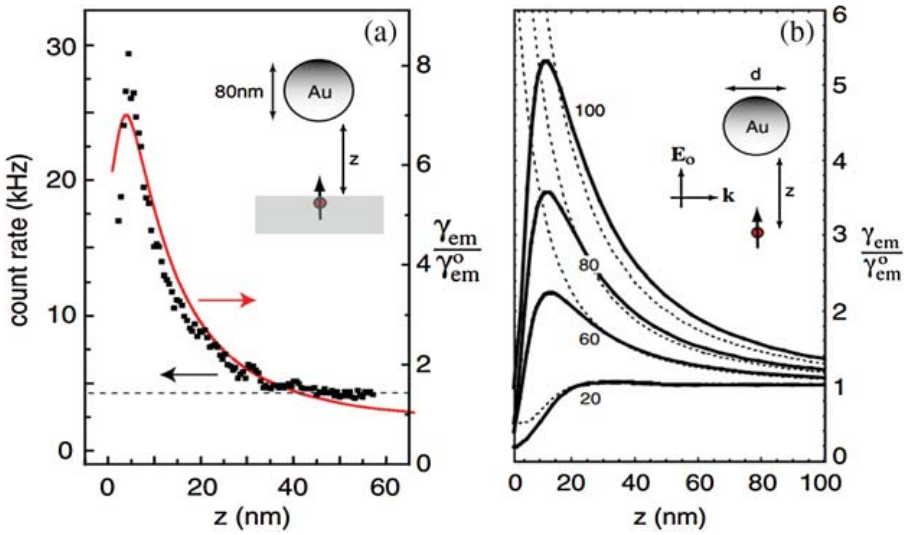


**Figure 3.20** (a) Fluorescence emission rate in experiments (dotted line) and the calculated curve in theory (solid line) as a function of the particle–surface distance. (b) Normalized fluorescence emission rate of a single molecule. The excitation wavelength is 650 nm, which coincides with the peak of the emission spectrum. The insets in (a) and (b) illustrate the system configuration in experiments and in simulation. Adapted from Ref. 38 with permission from the American Physical Society © 2006.

rate is normalized with its free space without a nanoparticle. The distance dependence in Fig. 3.20(a) agrees that the fluorescent emission rate increases sharply when the distance drops to less than 10 nm. Likewise, the calculated excitation rate shows the same trends as that of the emission rate.[38] The increase is attributed to the enhanced local field. However, when the separation distance is further reduced, the multipolar modes have to be taken into account. As shown in Fig. 3.20(b), the solid curves indicate the result of accounting for higher multipole modes, and the dashed curves correspond to the dipole approximation. The dipole approximation fails to describe the excitation rate and fluorescence emission rate for short distances. The multipolar calculation confirms the observed emission processes.

### 3.5.2 Localized surface plasmon resonance sensing

The spectroscopic characteristic of LSRPs provides a critical component for sensing applications. A transmission approach to probe the extinction spectrum characteristics is shown in Fig. 3.21. Nanoparticle clusters are used to excite and enhance the LSPRs. The enhanced local fields improve the scattering spectrum from the sample.

A fiber bundle works in a reflecting configuration, given the nontransparent materials involved, as shown in Fig. 3.22. A beam of light passes through the center fiber and illuminates the sample surface. The light reflected from the sample is collected through the external radial fibers. In the transmission configuration, the peak values in the extinction coefficient spectrum are

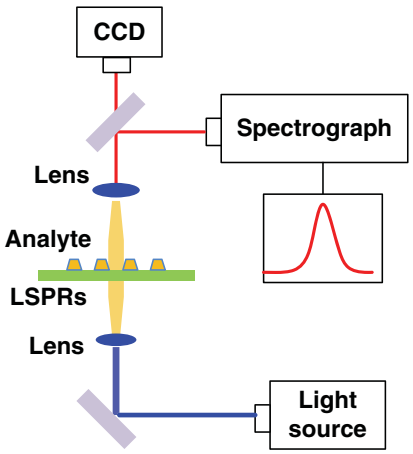


**Figure 3.21** Transmission configurations for sensing the extinction spectra of nanoparticle arrays

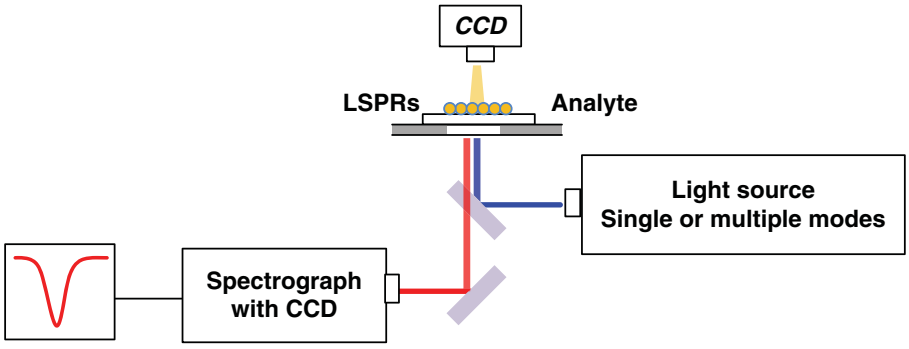


**Figure 3.22** Reflecting configurations for measuring the extinction spectra of nanoparticle arrays.

detected, while the minimum values of the reflective spectrum is detected in the reflecting geometry.[39] During the wavelength-shifting measurement, the LSPR extinction curves are collected. The drifting of the maximum peaks (or minimal value) is associated with the change in the local dielectric environment. In these conditions, the relationship described in Eq. (3.35) has been expanded to sensing proteins, antibodies, and other biological molecules.

To measure the surface-enhanced Raman scattering of a single nanoparticle or tiny area, a dark-field light-scattering method has proved to be extremely powerful. As shown in Fig. 3.23, one microscope objective with a high numerical aperture concentrates the excitation light onto the sample, and another microscope objective with a lower numerical aperture objective collects the scattering light from below. When a dark-field microscope objective is used to collect the LSPR spectra, it simultaneously guides the excitation light to the sample and collects the transmitted or scattered light from the sample.

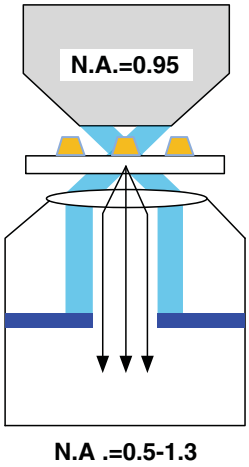


**Figure 3.23** Dark-field scattering experimental setup for measuring single-nanoparticle scattering spectra.

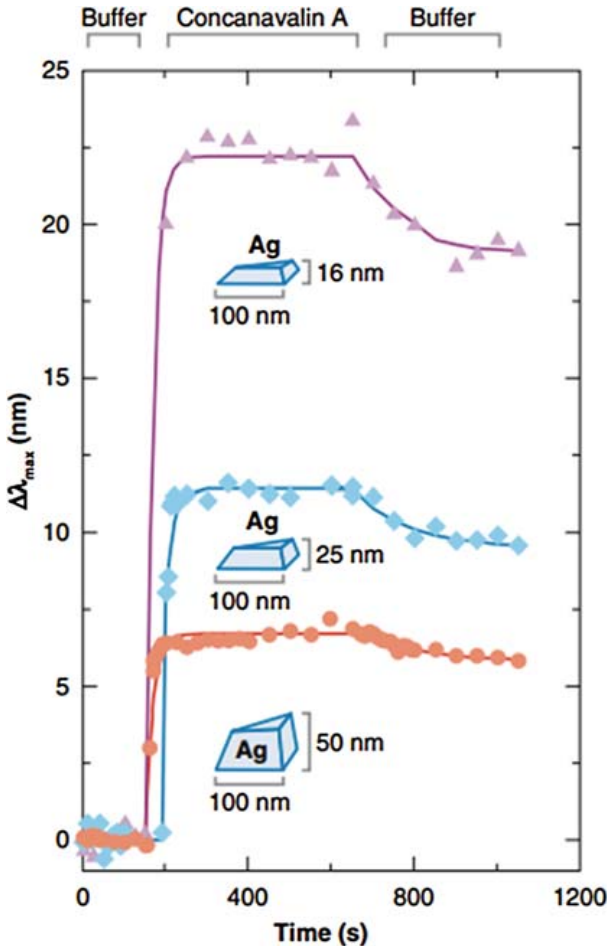


**Figure 3.24** Real-time responses of LSPRs in mannose-functionalized silver nanoparticles with different heights of 19-μM concanavalin A. Reproduced from Ref. 40 with permission from the American Chemical Society © 2004.

SERS has been demonstrated to be a sensitive and selective sensing method for the tracing detection of biological molecules. It provides greatly enhanced Raman signals from analyte molecules that have been adsorbed onto certain specially prepared metallic surfaces. During wavelength-scanning SERS spectroscopy, a specimen is excited by a laser with specific wavelengths, and the Raman-scattered spectrum is detected by a spectrometer. The measurements are often performed in an epi-illumination configuration co-operated with a microscope objective.[40] Figure 3.24 shows the wavelength shifting for functionalized nanoparticles with different thicknesses of concanavalin A. The changes of the shifting wavelength of LSPRs reveal the real-time kinetic response of the sample.[40]

Although the LSPR method offers promising features and potential applications for the development of LSPR-based biosensors, some issues must be addressed before practical activities are efficiently solved, e.g., improvements in the detection capability, multiplexing, and sensitivity, as well as integration of LSPRs with identification techniques.

## References


1. S. A. Maier, *Plasmonics: Fundamentals and Applications*. Springer, New York (2007).
2. C. F. Bohren and D. R. Huffman, *Absorption and Scattering of Light by Small Particles*, 1st ed., John Wiley & Sons, New York (1983).
3. S. Link and M. A. El-Sayed, "Shape and size dependence of radiative, non-radiative and photothermal properties of gold nanocrystals," *Int. Rev. Phys. Chem.* **19**, 409–453 (2000).
4. L. D. Landau et al., *Electrodynamics of Continuous Media*, Pergamon, Oxford, UK (1984).
5. M. I. Stockman, "Nanoplasmonics: past, present, and glimpse into future," *Optics Express* **19**, 22029 (2011).
6. L. Novotny and B. Hecht, *Principles of Nano-Optics*, p. 405, Cambridge University Press, Cambridge, UK (2006).
7. S. K. Ghosh and T. Pal, "Interparticle Coupling Effect on the Surface Plasmon Resonance of Gold Nanoparticles: From Theory to Applications," *Chem. Rev.* **107**, 4797–4862 (2007).
8. K. A. Willets and R. P. Van Duyne, "Localized Surface Plasmon Resonance Spectroscopy and Sensing," *Ann. Rev. Phys. Chem*. **58**, 267–297 (2007).
9. E. Petryayeva and U. J. Krull, "Localized surface plasmon resonance: Nanostructures, bioassays and biosensing-A review." *Analytica Chimica Acta*. **706**, 8–24 (2011).
10. K. L. Kelly, E. Coronado, L. Zhao, and G. Schatz, "The optical properties of metal nanoparticles: the influence of size, shape, and dielectric environment," *J. Phys. Chem. B* **107**, 668–77 (2003).

11. J. D. Jackson, *Classical Electrodynamics*, 3rd ed., John Wiley & Sons, New York (1999).
12. S. Hayashi and T. Okamoto, "Plasmonics: visit the past to know the future," *J. Phys. D: Appl. Phys.* **45**, 433001 (2012).
13. C. Sönnichsen et al., "Drastic reduction of plasmon damping in gold nanorods," *Phys. Rev. Lett.* **88**, 077402 (2002).
14. X. Huang and M. A. El-Sayed, "Gold nanoparticles: Optical properties and implementations in cancer diagnosis and photothermal therapy." *J. Adv. Res.* **1**, 13–28 (2010).
15. C. Sönnichsen et al., "Plasmon resonances in large noble-metal clusters." *New J. Physics* **4**, 93 (2002).
16. E. Dulkeith et al, "Fluorescence Quenching of Dye Molecules near Gold Nanoparticles: Radiative and Nonradiative Effects." *Phys. Rev. Lett.* **89**, 203002 (2002).
17. S. Kühn et al., "Enhancement of Single-Molecule Fluorescence Using a Gold Nanoparticle as an Optical Nanoantenna." *Phys. Rev. Lett.* **97**, 017402 (2006).
18. L. Tsang, J. A. Kong, and K. H. Ding, *Scattering of Electromagnetic Waves: Theories and Applications*, p. 12, John Wiley & Sons, New York (2000).
19. U. Kreibig and M. Vollmer, *Optical Properties of Metal Clusters*, Springer. Berlin (1995).
20. M. Quinten, *Optical Properties of Nanoparticle Systems*, Wiley-VCH, Weinheim, Germany (2011).
21. J. Pérez-Juste, I. Pastoriza-Santos, L. M. Liz-Marzán, and P. Mulvaney, "Gold nanorods: Synthesis, characterization and applications," *Coordination Chem. Rev.* **249**, 1870–1901 (2005).
22. U. Kreibig and C. V. Fragstein, "The Limitation of Electron Mean Free Path in Small Silver Particles," *Z. Physik* **224**, 307–323 (1969).
23. S. Link and M. A. El-Sayed, "Spectral properties and relaxation dynamics of surface plasmon electronic oscillations in gold and silver nano-dots and nano-rods," *J. Phys. Chem. B* **103**, 8410–8426 (1999).
24. M. Meier and A. Wokaun, "Enhanced fields on large metal particles: dynamic depolarization," *Opt. Lett.* **8**, 581–583 (1983).
25. H. Kuwata et al., "Resonant light scattering from metal nanoparticles: Practical analysis beyond Rayleigh approximation," *Appl. Phys. Lett.* **83**, 4625–4627 (2003).
26. L. S. Jung et al., "Quantitative interpretation of the response of surface plasmon resonance sensors to adsorbed films," *Langmuir* **14**, 5636–5648 (1998).
27. A. J. Haes and R. P. Van Duyne, "A nanoscale optical biosensor: sensitivity and selectivity of an approach based on the localized surface